Journal of Materials Chemistry A

PAPER

View Article Online
View Journal | View Issue

Cite this: J. Mater. Chem. A, 2018, 6, 22940

Comb-shaped sulfonated poly(ether ether ketone) as a cation exchange membrane for electrodialysis in acid recovery

Liang Wang, *[a] Minghui Liu,[ab] Junhua Zhao,[c] Yinlin Lei*[c] and Nanwen Li *[b]

To produce a cation exchange membrane (CEM) with high permselectivity and proton flux for electrodialysis (ED), a series of comb-shaped sulfonated poly(ether ether ketone) (SPEEK) membranes with long alkyl (butyl and octyl) side chains were synthesized using 1,1′-carbonyldiimidazole (CDI) as an activating reagent. The degree of substitution can be easily controlled by controlling the added amounts of CDI and reagents. The chemical structures were confirmed using a ^{1}H NMR technique. Transparent and tough membranes were prepared by solution casting. A well-defined hydrophilic–hydrophobic separation was achieved, as confirmed by small-angle X-ray scattering (SAXS). The comb-shaped membranes with the well-defined hydrophilic–hydrophobic separation effectively allow the transport of H^+, so higher H^+ flux is achieved in the ED process with the comb-shaped SPEEK membranes than that obtained with the SPEEK membrane despite the higher membrane resistance resulting from the lower ion-exchange capacity and lower water uptake. Interestingly, the lower swelling ratio of the comb-shaped membranes can block Fe^{2+} transport through the membranes. Thus, the comb-shaped membranes show much higher H^+/Fe^{2+} permselectivity than the pristine SPEEK membrane. The highest H^+ flux of 2.41×10^{-7} mol cm^{-2} s^{-1} and H^+/Fe^{2+} permselectivity of 32.13 are achieved for the SPEEK membrane with 30% substitution by octyl side chains. The performance is comparable with and even better than that of a commercial monovalent CEM from ASTOM. Considering the excellent thermal stability and mechanical properties, the comb-shaped SPEEK membranes are promising CEM materials for ED in acid recovery.

Received 8th September 2018
Accepted 15th October 2018

DOI: 10.1039/c8ta08718k

rsc.li/materials-a

Introduction

Wastewater treatment has become a worldwide problem with the development of industrialization. During industrial processes such as smelting, electroplating, mining, and metal surface treatment, inorganic acids are needed for metal surface cleaning or metal leaching, which generates a lot of waste acid containing metal ions, such as Fe^{2+}, Zn^{2+}, and Cu^{2+}.[1–4] If the wastewater from acid washing is directly discharged into the environment without treatment, it causes serious environmental problems, such as water and soil pollution.[5–8] Waste acid recovery and treatment methods mainly include electrodialysis (ED),[9,10] diffusion dialysis,[11,12] neutralization oxidation,[13] and distillation concentration.[14] Diffusion dialysis is a separation process where the concentration difference is the driving force for waste acid recovery, but the concentration of acid recovered and the efficiency of waste acid recovery are not sufficiently high. Therefore, a direct current (DC) electric field is used as the driving force to recover and treat the wastewater from acid washing, that is, ED.[15,16] Compared with other traditional treatment methods, industrial effluent treatment by ED is a reasonable choice considering its environmental friendliness, non-polluting nature, and high recovery efficiency.[17] At present, many studies have shown that the cation exchange membrane (CEM) is the key component of ED in acid recovery owing to its high separation efficiency.[18,19] However, the biggest challenge in the waste acid recovery ED process is how to obtain a CEM with both high proton permeability and high permselectivity.[20,21]

CEMs prepared from sulfonated polystyrene typically exhibit low permselectivity and thus fail to meet the requirements of the ED separation process in acid recovery.[22] Generally, improvement of the permselectivity can be achieved by increasing the proton permeability and decreasing the metal ion permeability during the ED process. The key to proton transport in CEMs is believed to be nanochannels that contain sulfonic acid groups, through which hydrated protons can efficiently pass.[23] Several approaches to form CEM nanochannels for fuel cell applications have been investigated to

[a]State Key Laboratory of Separation Membranes and Membrane Processes, School of Environmental and Chemical Engineering, Tianjin Polytechnic University, Tianjin 300387, China. E-mail: mashi7822@163.com

[b]State Key Laboratory of Coal Conversion, Institute of Coal Chemistry, Chinese Academy of Sciences, Taiyuan 030001, China. E-mail: linanwen@sxicc.ac.cn

[c]College of Chemical & Material Engineering, Quzhou University, Quzhou 324000, China. E-mail: nblaolei@163.com

improve proton transport, such as changing the acidity and position of the sulfonic acid groups and controlling the membrane morphology by forming block copolymer architectures.[23,24] However, these strategies are not used to prepare CEMs for ED applications owing to the complicated synthesis process and thus high cost. Researchers have focused on blocking metal ions to increase the CEM permeability during the ED process. For example, Sata and co-workers[25–27] prepared a series of acid–base complex CEMs based on Nafion and polypyrrole in which the dense layer can increase the monovalent/divalent cation selectivity of the membrane. Ge *et al.*[28] reported that membranes containing H^+ transfer channels constructed with acid–base pairs can be used for treatment of zinc hydrometallurgy effluents. Methods involving narrowing the pore size of the membrane by chemical crosslinking,[29] using the Donnan exclusion effect,[30] and blocking multicharge metal ions by introducing blockers[31] have also been developed to reduce the multivalent ion flux. However, these approaches only have limited success and generally lead to reduction of the proton or monovalent cation permeability.

Generally, the proton transport in PEMs is of great importance for their application in electrochemical devices, such as fuel cells, water electrolyzers, and flow batteries, as well as electrodialysis in water treatment. The formation of ion-conducting nanochannels in membranes can greatly increase the ionic conductivity of PEMs, leading to the improved performance of the above electrochemical devices.[32,33] Many possible strategies for obtaining well-defined nanochannel morphologies in membranes have been proposed, such as rational design of block or comb-shaped polymer architectures. Based on the previous reports,[34,35] the proton transport properties of comb-shaped PEMs can be readily tuned by adjusting the length and density of grafted chains as well as the nature of grafted chains. Recently, Lin *et al.*[36] synthesized a series of comb-shaped sulfonated poly(ether ether ketone) (SPEEK) membranes by RAFT polymerization of sodium *p*-styrenesulfonate. Thus, the hydrophobic side chains (sodium polystyrenesulfonate) were grafted onto the PEEK polymer backbones. The H^+ permeability of the obtained comb-shaped PEMs was measured under different current densities, which was much higher than that of the control sample (SPEEK). However, the synthetic procedure of these comb-shaped PEMs is complicated, which includes multi-step reactions and tedious purification. More importantly, the permselectivity of these comb-shaped PEMs in acid recovery was not investigated.

Herein, comb-shaped SPEEK membranes were designed and prepared using the 1,1′-carbonyldiimidazole (CDI)-catalysed sulfonamide formation reaction. It has been reported that the comb-shaped architecture with long alkyl chains can induce hydrophilic–hydrophobic separation in the anion exchange membrane (AEM).[37,38] Therefore, the comb-shaped architecture of SPEEK is expected to produce hydrophilic–hydrophobic separation, and thus enhance proton transport for ED application in acid recovery without sacrificing the permselectivity. A detailed investigation of the properties of comb-shaped SPEEK membranes with different alkyl side chain lengths was performed. Their water uptake (WU), swelling ratios (SR), proton permeability, and microphase-separated structures were determined and compared with those of pristine SPEEK and commercial CEMs.

Experimental

Materials

Anion exchange membranes (AEMs) were acquired from Liaoning Yi Chen Membrane Technology Co., Ltd (Liaoning, China) and the commercial membranes used in the electrodialysis experiments were CIMS (ASTOM Co., Japan). PEEK (450 P, MW = 28 800 g mol^{-1}) was obtained from Sigma Aldrich. 1,1′-Carbonyldiimidazole (CDI), butyl amine and octyl amine were purchased from Energy Chemical (Shanghai, China). Dimethyl sulfoxide (DMSO), ferrous sulfate heptahydrate ($FeSO_4 \cdot 7H_2O$) and other chemical reagents were obtained from Sinopharm Chemical Reagent Co., Ltd. They were of analytical grade and used without further purification.

Synthesis of SPEEK

20 g PEEK particles were gradually added to 400 mL concentrated sulfuric acid with vigorous mechanical stirring in a three-neck flask. After the complete dissolution of the PEEK particles, the reaction mixture was heated at 50 °C for 5 h. After the reaction was completed, the polymer solution was then cooled in an ice water bath to terminate the reaction and the sulfonated polymer was recovered by pouring the polymer solution into a large excess of ice water. The polymer was repeatedly washed with deionized water until the pH was neutral and dried under vacuum at 80 °C for 24 h. Finally, we obtained the yellow SPEEK polymer. The degree of sulfonation was determined to be 64% from ^{1}H NMR spectra.

Synthesis of butyl amine-SPEEK (4C-*x*-SPEEK) and octyl amine-SPEEK (8C-*x*-SPEEK)

Here, we will describe the process for preparation of 4C-30-SPEEK. The procedure for synthesis of 8C-*x*-SPEEK was the same as that for 4C-*x*-SPEEK except that octyl amine was used rather than butyl amine, as shown in Scheme 1. SPEEK (2 g, 3.78 mmol for $-SO_3H$ groups) was dissolved in 20 mL DMSO, and CDI (0.34 g, 2.08 mmol, with respect to the $-SO_3H$ groups of SPEEK) was added at room temperature. The reaction initially produced CO_2. The solution was allowed to reflux at 60 °C for

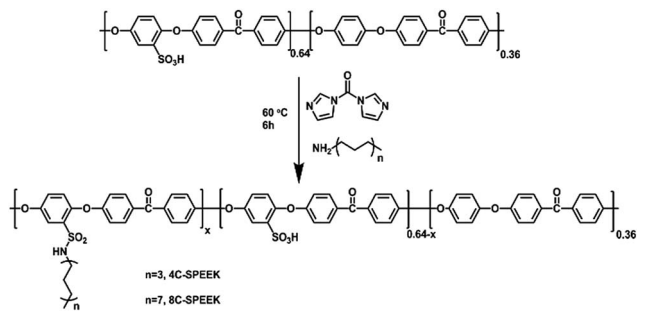

Scheme 1 Synthesis of 4C-*x* and 8C-*x* comb-shaped SPEEK.

3 h with stirring and then butyl amine (0.175 mL, 1.77 mmol) was added. After further reaction at 60 °C for 3 h, the polymer solution was cooled to ambient temperature and poured into diethyl ether with a small amount of methanol. The product was filtered and washed several times with deionized water and the 4C-SPEEK polymer was dried in a vacuum oven at 80 °C for 24 h.

Preparation of the ion exchange membranes

4C-SPEEK or 8C-SPEEK was dissolved in DMSO (8 wt%), and the solution was cast on a clean glass plate at 80 °C for 12 h. Immediately, the glass plate was then immersed into deionized water and the membrane automatically peeled off from the glass plate. According to the degree of substitution of butyl amine and octyl amine, the membranes were labeled 4C-10, 4C-20, 4C-30, 8C-10, 8C-20 and 8C-30, respectively. Before all the tests, the membranes were immersed in 0.5 M H_2SO_4 at room temperature for one day and then repeatedly washed with deionized water.

Membrane characterization

The ^{1}H NMR spectra were recorded with a Bruker AVANCE 400 instrument (400 MHz) using DMSO-d_6 as the solvent. The tensile property measurements were carried out with an INSTRON-5869 material testing instrument at ambient temperature with a uniform speed of 5 mm min^{-1}. After the measurements were completed, the tensile strength, Young's modulus and elongation at break values were recorded. Small-angle X-ray scattering (SAXS) of the dry membranes was performed with a SAXS Nanostart instrument (Bruker Co., USA) equipped with a CuKα slit-collimated X-ray source operating at 40 kV and 50 mA. The thermal stabilities of the modified membranes were measured by thermogravimetric analysis (TGA) under a nitrogen atmosphere with a TG-DTASDT Q600 analyser at a heating rate of 10 °C min^{-1}. Before all the measurements, the membranes were cut into 1 cm × 4 cm pieces and dried in a vacuum at 60 °C for 12 h.

Water uptake, swelling ratio and IEC

Water uptake (WU) was measured to investigate the membrane hydrophilicity. Before the test, the membrane sample was cut into a 1 cm × 3 cm piece and immersed in deionized water at 25 °C for 24 h. Afterwards, the water on the surface was mopped up with tissue paper and the sample was weighed in the wet state (W_{wet}); the dry weight of the membrane (W_{dry}) was determined after drying the membrane under vacuum at 60 °C for 24 h. Water uptake could be calculated as follows:

$$\mathrm{WU} = \frac{W_{wet} - W_{dry}}{W_{dry}} \times 100\%$$

The swelling ratio of the membrane was measured using the difference in length between the dry (L_{dry}) and wet (L_{wet}) membrane, which was calculated based on the following equation:

$$\mathrm{SR} = \frac{L_{wet} - L_{dry}}{L_{dry}} \times 100\%$$

Ion exchange capacity (IEC) values of the membranes were determined by back titration and ^{1}H NMR analysis according to a previously reported method.[39] A weighed piece of membrane was immersed in a 0.1 M NaCl aqueous solution for 24 h to replace H^+ with Na^+. The HCl released by the ion exchange was titrated with a standard 0.01 M NaOH solution using phenolphthalein as an indicator. Moreover, the IEC values were further confirmed using ^{1}H NMR spectra, as shown in Fig. 3. The IEC was expressed as the milliequivalents (meq.) of (–SO_3H)/g of the dry polymer and obtained using the following equation:

$$\mathrm{IEC} = \frac{V_{NaOH} \times C_{NaOH}}{m}$$

Proton conductivity measurements

The proton conductivity (σ, S cm^{-1}) of each membrane coupon (size: 1 cm × 4 cm) was obtained using $\sigma = d/L_sW_sR$ (d is the distance between reference electrodes, and L_s and W_s are the thickness and width of the membrane, respectively). The resistance value (R) was measured over the frequency range from 100 mHz to 100 kHz by four-point probe alternating current (ac) impedance spectroscopy using an electrode system connected to an impedance/gain-phase analyzer (Solartron 1260) and an electrochemical interface (Solartron 1287, Farnborough Hampshire, ONR, UK). The membranes were sandwiched between two pairs of gold-plated electrodes. The conductivity measurements under completely hydrated conditions were carried out with the cell immersed in liquid water. The impedance of each sample was measured at least three times to ensure reproducibility of the data.

Electrodialysis tests

All the electrodialysis tests were carried out in a H^+/Fe^{2+} system to measure the ion flux and permselectivity. As shown in Fig. 1, the electrodialysis installation consisted of four compartments (an anode cell, a cathode cell, a concentrated cell and a diluted cell) separated by two pieces of anion exchange membranes and one piece of the 4C-x or 8C-x membrane. The diluted cell was

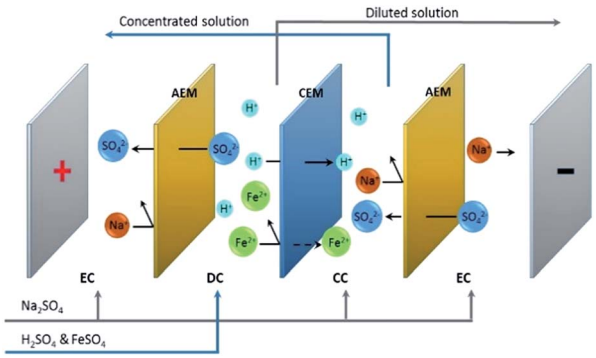

Fig. 1 Schematic principle of electrodialysis.

filled with 40 mL of 0.5 mol L^{-1} $FeSO_4$ in 0.25 mol L^{-1} H_2SO_4, and the concentrated cell was filled with 20 mL of 0.3 mol L^{-1} Na_2SO_4. The electrode cells were filled with 40 mL of 0.3 mol L^{-1} Na_2SO_4. The effective area of the membrane between the two electrodes was 4.90 cm^2, and the electrodes were made of titanium coated with ruthenium. A certain current density was applied to the system and electrodialysis was performed for 1 h. The solution of the concentrated cell was then collected and the concentration of H^+ and Fe^{2+} was determined by conventional titration. In order to reduce the error caused by the operation, three electrodialysis tests for each membrane were performed in parallel, and the average values have been shown.

The H^+ and Fe^{2+} ion fluxes in the concentrated cell after electrodialysis could be calculated as follows:

$$J_{H^+} = \frac{\Delta C_{H^+} V}{A_m t}$$

$$J_{Fe^{2+}} = \frac{\Delta C_{Fe^{2+}} V}{A_m t}$$

where J_H^+ and J_{Fe}^{2+} are the H^+ and Fe^{2+} ion fluxes after electrodialysis in mol cm^{-2} s^{-1}, and ΔC_H^+ and ΔC_{Fe}^{2+} are the H^+ and Fe^{2+} concentration in the concentrated cell, respectively. V is the volume of the solution in the concentrated cell and A_m is the effective area of the membrane, which was 4.9 cm^2.

The permselectivity for H^+/Fe^{2+} in this study was simply calculated as the ratio of ion fluxes between H^+ and Fe^{2+} because the initial concentrations of the two ions were the same in the diluted cell.[40,41]

Current–voltage (*I–V*) curves

Current–voltage curves were measured using a four-compartment installation (an anode cell, a cathode cell and two test cells) and a direct current which gradually increased was applied to the system. In this system, 0.3 M Na_2SO_4 and 0.5 M H_2SO_4 were used as the electrolyte solution and test solution, respectively (Fig. 2). The effective area of the membrane was 7.07 cm^2 and the electrodes were made of titanium coated with ruthenium. At the same time, a pair of Ag–AgCl electrodes was used to connect the voltage ammeter, provide current and measure the voltage. To eliminate the possible effect of the electrode reactions on the experimental results, a blank test without the membrane arranged between the pair of electrodes in the test solution was carried out.[28,42,43] All the membrane samples were tested in triplicate and the average values have been shown in discussion.

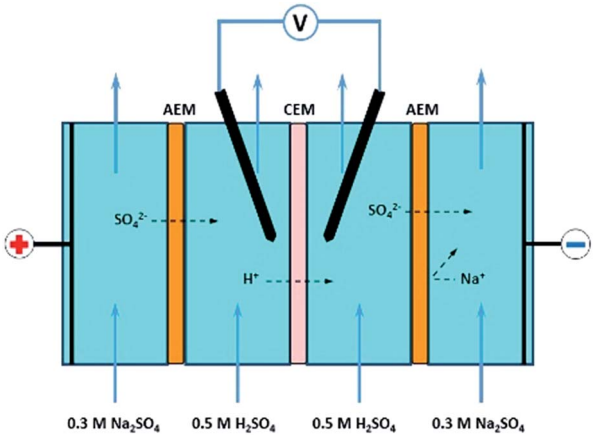

Fig. 2 Schematic principle of current–voltage curve measurement.

Results and discussion

Synthesis and characterization of the polymer

Generally, CDI is used as an activating agent for the reaction between sulfonic acid groups and primary amine reagents. Thus, this typical reaction has been developed for the quantitative post-modification of the sulfonated polymer.[44,45] The SPEEK polymer has been prepared according to previous reports and has a degree of sulfonation of 64% which was confirmed by the ^1H NMR technique (Fig. 3(a)). As shown in Scheme 1, firstly, SPEEK reacted with CDI to form sulphonamide, and then *n*-butyl amine or *n*-octyl amine attached to produce the functionalized SPEEK copolymers 4C-*x* or 8C-*x*, respectively (where *x* is the degree of substitution of the alkyl side chains). The degree of substitution of the polymer was controlled using the amount of CDI reagent added. However, the highest degree of substitution that can be achieved is 50% according to the reaction mechanism.

The chemical structures of 4C-*x* and 8C-*x* were determined using ^1H NMR spectra. The ^1H NMR spectra are shown in Fig. 3(b); the appearance of new peaks corresponding to the methylene protons of 4C-*x* and 8C-*x* in the range of 1.30–2.75 ppm and the methyl proton peak at 0.83 ppm indicate successful formation of the comb-shaped sulfonamide alkyl chain. The degrees of substitution were further determined using the integral ratios between the methyl groups and aromatic protons ($H_{1'}$) which are close to the sulfonic acid groups. These values range from 10–30% which agrees well with the theoretical values. Moreover, the 4C-*x* and 8C-*x* exhibited excellent solubility in DMSO, NMP and DMF. The transparent and tough membranes were obtained by solution casting of their DMSO solution on glass plates, as shown in Fig. 4.

Mechanical properties and thermal stability

The mechanical properties of all the membranes were measured in dry and wet states at room temperature, and the results are listed in Table 1. Interestingly, the comb-shaped 4C-*x* and 8C-*x* membranes exhibited mechanical properties with a tensile strength of 65.9–94.2 MPa and a Young's modulus of 836–1380 MPa in dry state. These values were much higher than that of the pristine SPEEK membrane (tensile strength of 60.6 MPa and Young's modulus of 668 MPa). It is assumed that the hydrophobic alkyl chains in the comb-shaped architecture would restrict the water absorption of membranes (which will be shown below) and thus decrease the plasticizing effect of water on the mechanical strength of the resulting 4C-*x* and 8C-*x* membranes. Additionally, the elongation at break of comb-shaped 4C-*x* and 8C-*x* membranes in the range of 51–110%

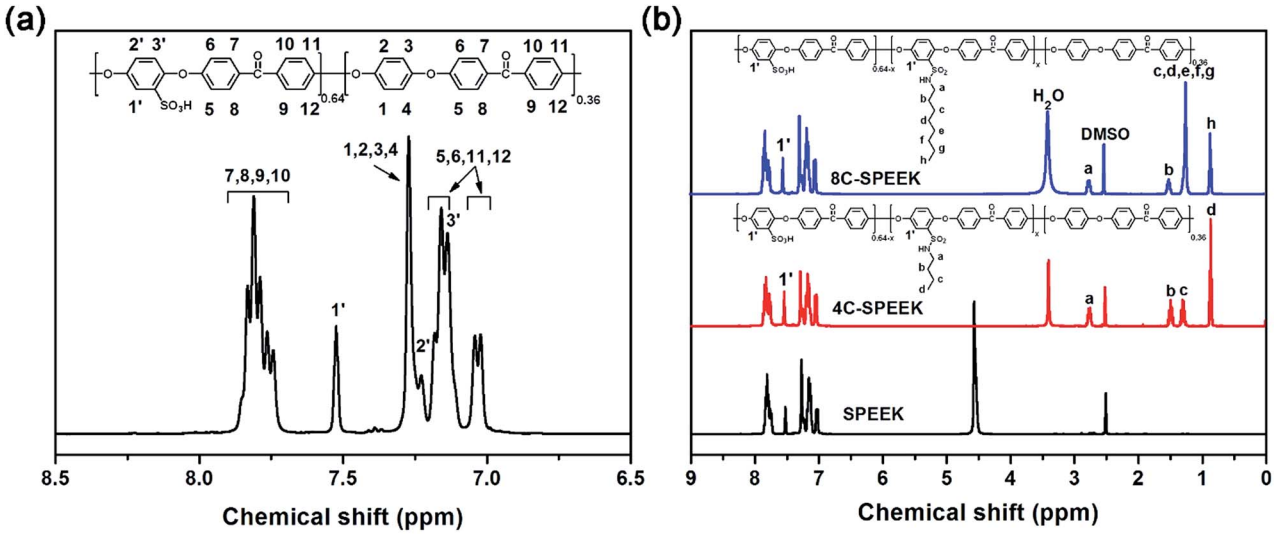

Fig. 3 ^{1}H NMR spectra of the SPEEK, 4C-SPEEK, and 8C-SPEEK in DMSO-d_6.

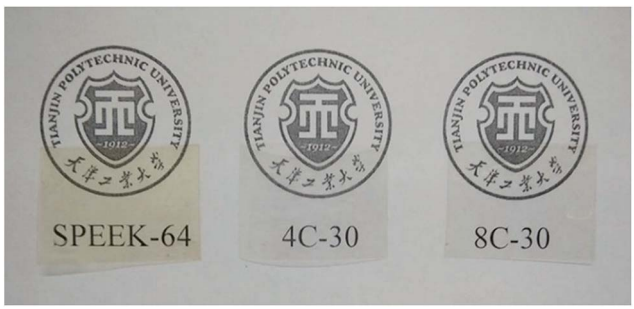

Fig. 4 Optical photographs of the pristine SPEEK, 4C-30 and 8C-30 membranes.

Table 1 Mechanical properties of membranes at room temperature

	Tensile strength (MPa)		Young's modulus (MPa)		Elongation at break (%)	
Membrane	Dry[a]	Wet[b]	Dry[a]	Wet[b]	Dry[a]	Wet[b]
SPEEK	60.6	40.3	668	585	130	168
4C-10	72.9	53.7	906	827	88	117
4C-20	85.5	65.6	1130	1039	60	90
4C-30	94.2	70.6	1380	1185	51	77
8C-10	65.9	46.8	836	733	110	133
8C-20	74.1	57.4	994	906	80	101
8C-30	80.8	64.3	1173	1050	62	95

[a] At 40% RH. [b] At 100% RH.

decreased with the increase of degree of substitution. Moreover, when the membranes were tested in wet condition, the tensile strength and Young's modulus of wet membranes were reduced, while the elongation at break was increased compared to that of dry samples. Thus, the mechanical strength of the obtained comb-shaped membranes is sufficient for their application in electrodialysis.

The thermal stabilities of the membranes were measured by TGA from 50 to 800 °C under a N_2 atmosphere. As shown in Fig. 5, the initial degradation stage observed at around 300–400 °C was associated with the thermal degradation of the sulfonic acid groups.[45] The second degradation stage starting at above 450 °C corresponds to the degradation of the alkyl side chains and polymer main chains. The results indicated that the comb-shaped membranes will maintain their excellent thermal stability for electrodialysis in acid recovery.

Morphological structure

Small-angle X-ray scattering (SAXS) was performed to characterize the morphological structure of the comb-shaped membranes. Generally, the characteristic ion-rich domain that contributed to the micro-phase separation in membranes can be observed from the appearance of the q peak in SAXS results.[46–48] As shown in Fig. 6, the 4C-30 and 8C-30 membranes

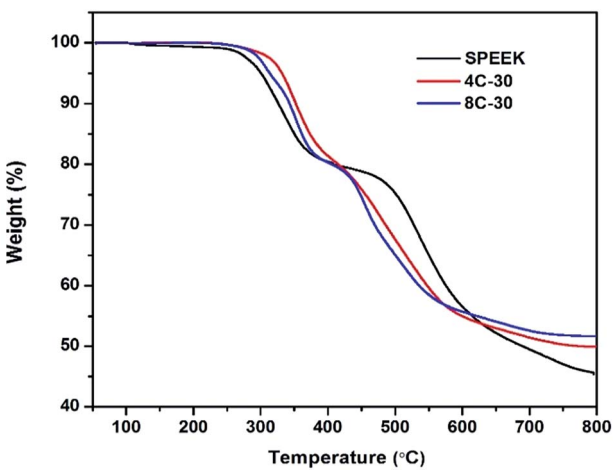

Fig. 5 TGA curves of the SPEEK, 4C-30 and 8C-30.

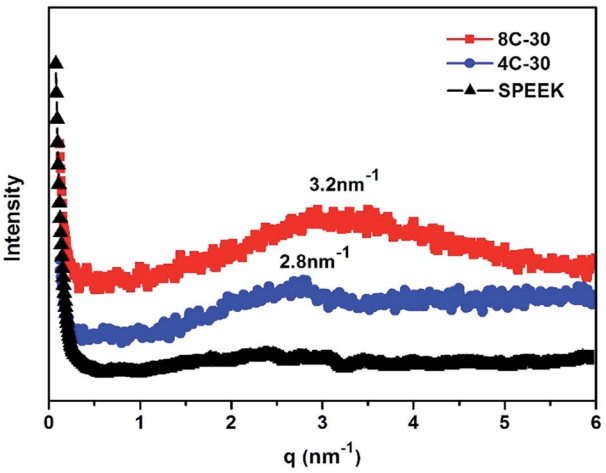

Fig. 6 SAXS profiles of the SPEEK, 4C-30 and 8C-30.

showed the ionomer peaks at ~3 nm^{-1}. However, there are no obvious peaks in the SAXS results for the pristine SPEEK membrane. This result indicated that the hydrophobic alkyl chains induced the formation of hydrophilic–hydrophobic phase separation in the comb-shaped membranes, as shown in our previous studies.[46,49] The ionomer peaks are located at q = 2.8 nm^{-1} and 3.2 nm^{-1} for the 4C-30 and 8C-30 membranes, respectively. Thus, the characteristic separation length scale values (d) calculated using the equation $d = 2\pi/q$ are 2.2 and 1.9 nm for the 4C-30 and 8C-30 membranes, respectively. With increasing length of the alkyl side chain, the micro-phase separation becomes more obvious because of the stronger hydrophobicity.

Water uptake (WU) and swelling ratio (SR) of membranes

Reasonable water uptake is beneficial for ion transport in CEMs; however, excessive water uptake will cause excessive swelling of the membrane and thus result in degradation of the mechanical properties.[50] Therefore, the comb-shaped architecture was developed in this study to enhance the ion transport without degradation of the mechanical properties, *e.g.* lower water uptake and swelling ratio. The water uptake and swelling ratio values of the 4C-x and 8C-x comb-shaped membranes were measured and compared with those of the pristine SPEEK membrane. As shown in Table 2, the water uptake (WU) (15.8–26.4%) and swelling ratio (SR) (7.1–10.7%) of the comb-shaped membranes were much lower than those of the pristine SPEEK membrane (WU = 30.8, SR = 12.7). Thus, the comb-shaped membranes have excellent mechanical properties. The titrated IEC values are very close to the calculated values from ^{1}H NMR. As expected, the water uptake decreased with increasing the degree of substitution in the comb-shaped membranes owing to the decreased IEC_W values. For example, the water uptake of 8C-x membrane decreased from 26.6% to 15.8% when the degree of substitution increased from 10% to 30%, *i.e.* the IEC_W values decreased from 1.81 to 1.49 meq. g^{-1}. Thus, lower water uptake resulted in lower swelling ratio, as shown in Fig. 7(b).

Proton conductivity

The proton conductivity values of the pristine SPEEK and comb-shaped membranes in water at 25 °C are listed in Table 2. For the comb-shaped membranes, an increase in proton conductivity values with IEC_W was observed. Similar to the water uptake, the membranes with higher IEC showed higher proton conductivity, as listed in Table 2. The effects of alkyl chain length and substitution degree are also consistent with the water uptake, where the hydration of the pristine SPEEK membrane with high IEC_W values resulted in excessive swelling and dilution of the ion concentration, thus decreasing IEC_V. Compared with the comb-shaped 4C-10 (IEC_W = 1.88 meq. g^{-1}) and 8C-10 (IEC_W = 1.81 meq. g^{-1}) membranes with similar IEC values and a smaller number of sulfonic acid groups per repeat unit, the pristine SPEEK membrane shows higher proton conductivity (IEC_W = 2.08 meq. g^{-1}), which indicates that the presence of more sulfonic acid groups along the polymer chain is more effective for proton conduction.

Current–voltage curves

Membrane resistance is a key parameter in the development of electrically driven membrane processes, and it determines the total energy consumption and total cost of the electrically driven membrane process. A suitable membrane resistance is beneficial for the electrodialysis process because it results in lower power loss, thereby increasing the productivity and reducing equipment operating costs. A current–voltage curve is

Table 2 The IEC, water uptake, swelling ratio and proton conductivity of the membranes

Membrane	IEC_W (meq. g^{-1}) Calcd[a]	IEC_W (meq. g^{-1}) Expt[b]	IEC_V[c] (meq. cm^{-3})	Water uptake (%)	Swelling ratio (%)	Thickness (μm)	Proton conductivity (S cm^{-1})
SPEEK-64	2.08	1.98	1.59	30.8	12.7	65	0.096
4C-10	1.88	1.74	1.48	28.4	10.7	67	0.084
4C-20	1.72	1.60	1.41	23.8	9.3	62	0.068
4C-30	1.57	1.47	1.35	17.3	7.8	63	0.055
8C-10	1.81	1.67	1.44	26.6	10.3	65	0.079
8C-20	1.64	1.51	1.37	20.1	8.9	60	0.063
8C-30	1.49	1.39	1.29	15.8	7.1	64	0.048

[a] Calculated from ^{1}H NMR. [b] Titrated IEC values. [c] Based on IEC_W[a] ($IEC_V = IEC_W/(1 + 0.01WU)$).

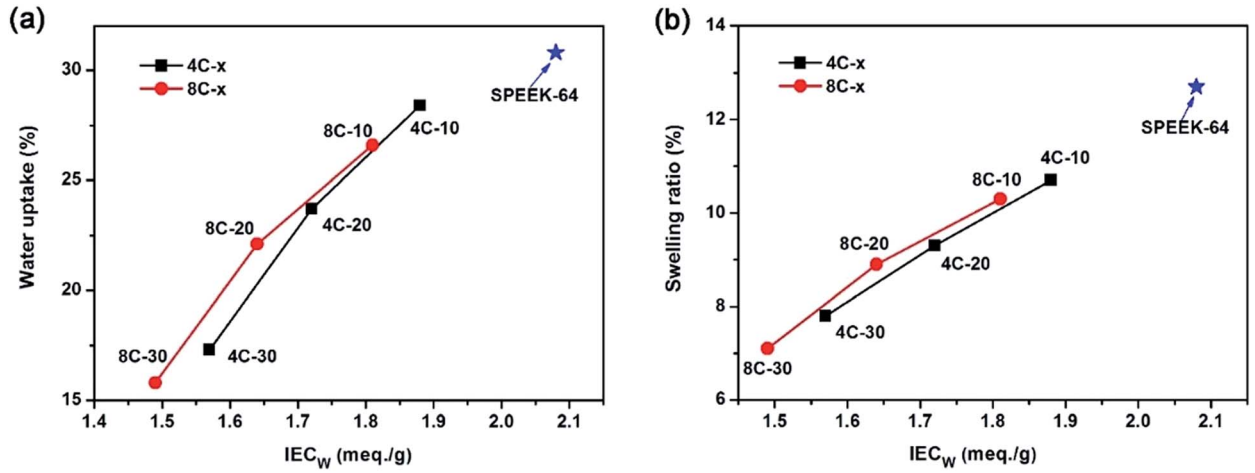

Fig. 7 The dependence of water uptake (a) and swelling ratio (b) on the IEC$_W$ values of 4C-*x*, 8C-*x* and SPEEK membranes.

generally used to investigate the membrane resistance and limiting current density (i_{lim}) which can be employed to determine the operating current density to avoid electrolysis of water in the electrodialysis process. Moreover, a lower operating current density than the limiting current density would decrease or prevent fouling in the equipment which is caused by concentration polarization. Thus, the current–voltage curves of the pristine SPEEK, and the comb-shaped 4C-*x* and 8C-*x* membranes were measured under the same testing conditions.

As shown in Fig. 8, the current–voltage curves of the membranes displayed the typical three-region model. The first region at low current densities ($i < i_{lim}$) is the ohmic region, which is caused by ion transport between the solution interface and the membrane. In this region, the potential drop on the membrane is directly proportional to the applied current, and the ohmic resistance (*i.e.*, membrane resistance) can be calculated from the slope of the ohmic region.[51] Subsequently, when the current density increases and approaches the limiting current density, the rate of ion transport across the membrane will increase, and the concentration of ions close to the interface will rapidly decrease. Thus, an increase in the resistance results in a smaller slope. This region is called the plateau region, which indicates the maximum current density that can be applied in the electrodialysis process.[52] The limiting current density can be estimated using the intersection of the ohmic region and the plateau region. However, as the current density was further increased, the velocity of the charged ions across the membrane cannot meet the requirements of the operating current, so concentration polarization in the solution and hydrolysis occur.[53] Thus, a high slope is observed in this region, *i.e.* the over-limiting region.[54]

As discussed above, the membrane resistances of the pristine SPEEK and comb-shaped membranes have been calculated, and the results are shown in Table 3. After modification with alkyl chains, the membrane resistances of the comb-shaped membrane are in the range of 1.38–2.57 Ω cm^2. These

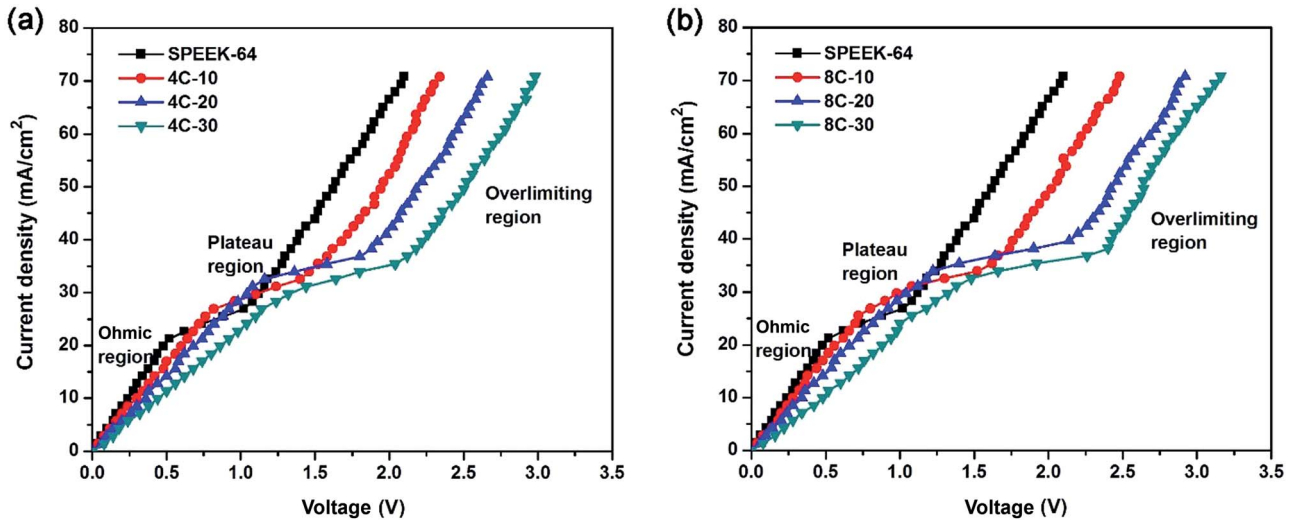

Fig. 8 Current–voltage curves of the SPEEK, 4C-*x* (a) and 8C-*x* membranes (b).

Table 3 The area resistance and limiting current density of membranes

Membrane	IEC_W (meq. g^{-1})	Area resistance (Ω cm^2)	Limiting current density (mA cm^{-2})
SPEEK-64	2.08	1.38	21.23
4C-10	1.88	1.51	25.47
4C-20	1.72	1.75	29.72
4C-30	1.57	2.34	31.14
8C-10	1.81	1.61	26.89
8C-20	1.64	1.86	32.46
8C-30	1.49	2.57	33.97

values are higher than the membrane resistance of the pristine SPEEK membrane (1.28 Ω cm^2), probably because of the lower IEC values. Thus, the membrane resistance increases with increasing degree of substitution of alkyl chains. It is worth noting that compared with the pristine SPEEK membrane, the limiting current densities of the comb-shaped membranes are increased significantly from 21.23 mA cm^{-2} to 33.97 mA cm^{-2} under the same experimental conditions. Because the pristine SPEEK membrane lacks sufficient channels to provide more ion transport and satisfy the demand of current conduction, a low limiting current density will result in electrolysis of water. In contrast, after modification with alkyl chains to form comb-shaped architectures, the membranes show higher limiting current densities, owing to the well-defined hydrophilic/hydrophobic micro-phase separation enhancing the H^+ transport. Therefore, the suitable area resistance and high limiting current density values could meet various water quality requirements and the membranes can be used in the electrodialysis process.

Electrodialysis tests

To investigate the separation performance of monovalent/divalent cations, a series of electrodialysis tests of the comb-shaped membranes were performed in the $H_2SO_4/FeSO_4$ system to simulate potential application systems. An operating current density of 10 mA cm^{-2} which is lower than the limiting current density of the membranes was used to avoid water electrolysis and incipient precipitation of $Fe(OH)_2$ in the diluted chamber.[41] As shown in Fig. 9, all the comb-shaped membranes exhibited higher H^+ flux than that of the pristine SPEEK

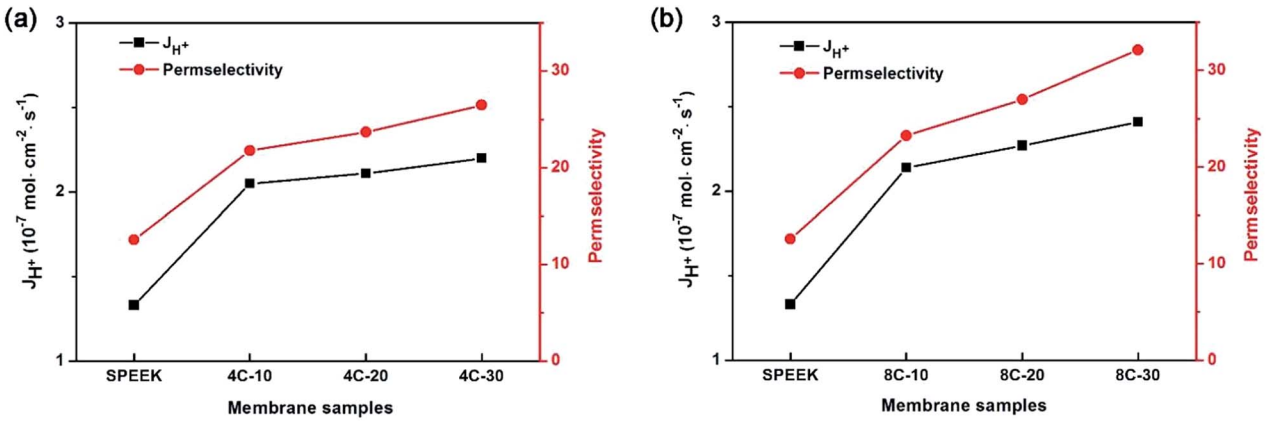

Fig. 9 Ion flux and permselectivity of the pristine SPEEK membrane and comb-shaped membranes with different degrees of substitution.

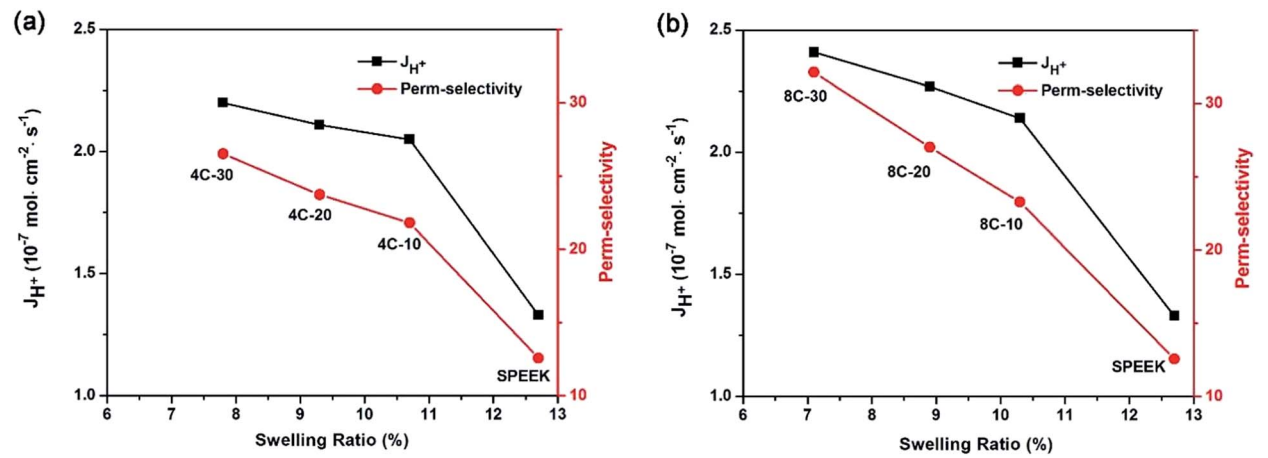

Fig. 10 A series of comb-shaped membranes with H^+ flux and permselectivity as a function of swelling ratio.

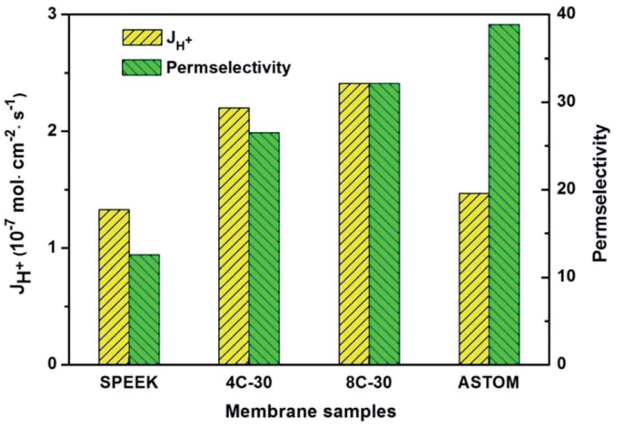

Fig. 11 Comparison of the pristine SPEEK membrane, comb-shaped membranes and ASTOM.

membrane. This can be attributed to the well-defined hydrophilic/hydrophobic separation, as confirmed by SAXS results, which enhanced the H^+ transport during the electrodialysis process.[55] Thus, the H^+ flux increases from 1.33 to 2.20 $\times$ 10^{-7} mol cm^{-2} s^{-1} when the degree of substitution by butyl alkyl chains increases from 10% to 30%, as shown in Fig. 9(a). These values are much higher than that of the pristine SPEEK membrane with a H^+ flux of 1.33 $\times$ 10^{-7} mol cm^{-2} s^{-1}. Interestingly, after modification with alkyl chains to form comb-shaped architectures, the membranes not only show higher H^+ flux but also higher H^+/Fe^{2+} permselectivity, as shown in Fig. 9. The highest permselectivity of 32.13 is achieved for the 8C-30 membrane, which also has the highest H^+ flux of 2.41 $\times$ 10^{-7} mol cm^{-2} s^{-1}. These values are much higher than those of the pristine SPEEK membrane having a permselectivity of 12.55 and a H^+ flux of 1.33 $\times$ 10^{-7} mol cm^{-2} s^{-1}. It is believed that the well-defined hydrophilic/hydrophobic separation can enhance the H^+ transport. However, the lower IEC values and thus the swelling ratio would effectively prevent Fe^{2+} transport through the membrane owing to the larger Stokes radius of Fe^{2+} than that of H^+.[56] Therefore, the well-defined comb-shaped membranes show higher H^+ flux and permselectivity with decreasing the swelling ratio, as shown in Fig. 10. These results indicate that the introduction of alkyl chains in the CEMs to form a comb-shaped architecture, and thus a well-defined hydrophilic–hydrophobic separation can overcome the trade-off effect between ion flux and permselectivity, which generally occurs in previously reported design strategies.[57,58]

Additionally, the 8C-30 membrane also showed higher H^+ flux and H^+/Fe^{2+} permselectivity than those of the 4C-30 membrane despite their similar IEC and swelling ratio values, as shown in Fig. 11. It is presumed that the 8C-30 membrane with longer alkyl chains would induce a more well-defined hydrophilic–hydrophobic separation than 4C-30. This result was confirmed by SAXS as discussed above, in which the 8C-30 membrane showed a sharper ionomer peak than the 4C-30 membrane. Compared with the performance of the commercial monovalent CEM from ASTOM which was characterized under the same testing conditions, the comb-shaped membranes still showed higher H^+ flux and comparable H^+/Fe^{2+} permeability. Further improvement of the permselectivity could be achieved by decreasing the swelling ratio such as by crosslinking, which will be reported in the future.

Finally, we compared the results for the comb-shaped membranes with those of other membranes used in ED processes for the recovery of acids reported in the literature and they are listed in Table 4. Compared with the other similar proton selective membranes, this comb-shaped membrane indicated that the proton permselectivity of a CEM can be greatly increased by grafting alkyl side chains. Furthermore, the comb-shaped membrane can maintain a high proton flux under a lower current density.

Conclusions

Comb-shaped SPEEK membranes have been successfully prepared by introduction of alkyl chains to typical SPEEK by the CDI activated addition reaction. A well-defined hydrophilic–hydrophobic separation is achieved, as confirmed by SAXS, where the comb-shaped membranes show obvious ionomer peaks. Thus, the comb-shaped membranes exhibit a suitable area resistance owing to the well-defined micro-phase separation despite their lower IEC and water uptake values than the SPEEK membrane. Thus, the limiting current densities of the comb-shaped membranes are higher than that of the SPEEK membrane. Electrodialysis test results indicate that the comb-shaped membranes exhibit higher H^+ fluxes in the range of 2.05–2.41 $\times$ 10^{-7} mol cm^{-2} s^{-1} than that of the pristine SPEEK

Table 4 Summary of membranes used in ED for the recovery of acids

Membranes	Current density (mA cm^{-2})	H^+ flux (mol cm^{-2} s^{-1})	Permselectivity	Ref.
Comb-shaped sulfonated poly(ether ether ketone) membranes	10	2.41 $\times$ 10^{-7}	32.13	This work
BPPO membranes with zwitterionic side chains	14	4.7 $\times$ 10^{-7}	23.5	59
Commercial CSO membrane	14	1.9 $\times$ 10^{-7}	3.52	59
SPSF porous supporting membranes with PEI or PVA	15	2.91 $\times$ 10^{-7}	20.78	60
PVA based CEMs using annealing treatment	30	2.8 $\times$ 10^{-7}	14.2	61
Flowsheet based on the combination of membrane processes and microporous hollow-fiber contactors	50	5.5 $\times$ 10^{-7}	9.5	62

membrane ($J_{H^+} = 1.33 \times 10^{-7}$ mol cm^{-2} s^{-1}). It is presumed that the well-defined hydrophilic/hydrophobic separation of the comb-shaped membranes enhances the transport of H^+ despite their lower IEC values. Thus, the H^+ ion flux significantly increases with increasing length of the alkyl side chains and degree of substitution by alkyl chains. Importantly, the lower IEC value, and thus the water uptake, results in the lower swelling ratio, which results in the lower Fe^{2+} leakage during the electrodialysis process owing to the larger Stokes radius of Fe^{2+} than that of H^+. Thus, excellent H^+/Fe^{2+} permselectivity is achieved for the comb-shaped membranes. Combined with the excellent thermal stability and mechanical properties, the comb-shaped SPEEK membranes are promising CEM materials that can be applied in ED for acid recovery.

Conflicts of interest

There are no conflicts to declare.

Acknowledgements

Financial support for this work was provided by the Autonomous Research Project of SKLCC, the National Natural Science Foundation of China (No. 51478314, 51638011, 51678408), the Science and Technology Plans of Tianjin [Grant No. 17PTSYJC00050 and 17ZYPTJC00060], the Hundred Talents Program of the Chinese Academy of Sciences, and the Hundred Talents Program of the Shanxi Province.

Notes and references

1 M. A. Shannon, P. W. Bohn, M. Elimelech, J. G. Georgiadis, B. J. Marinas and A. M. Mayes, *Nature*, 2008, **452**, 301–310.
2 D. W. Kolpin, E. T. Furlong, M. T. Meyer, E. M. Thurman, S. D. Zaugg, L. B. Barber and H. T. Buxton, *Environ. Sci. Technol.*, 2002, **36**, 1202–1211.
3 J. Y. Lee, C. H. Chen, S. Cheng and H. Y. Li, *Int. J. Environ. Sci. Technol.*, 2016, **13**, 65–76.
4 J. Chung, J. Chun, J. Lee, S. H. Lee, Y. J. Lee and S. W. Hong, *J. Hazard. Mater.*, 2012, **239**, 183–191.
5 J. Khan, B. P. Tripathi, A. Saxena and V. K. Shahi, *Electrochim. Acta*, 2007, **52**, 6719–6727.
6 D. H. Kim, *Desalination*, 2011, **270**, 1–8.
7 F. Smagghe, J. Mourgues, J. L. Escudier, T. Conte, J. Molinier and C. Malmary, *Bioresour. Technol.*, 1992, **39**, 185–189.
8 G. S. Gohil, V. V. Binsu and V. K. Shahi, *J. Membr. Sci.*, 2006, **280**, 210–218.
9 Y. X. Jia, F. J. Li, X. Chen and M. Wang, *Sep. Purif. Technol.*, 2018, **190**, 261–267.
10 L. Wang, Z. Li, Z. Xu, F. Zhang, J. E. Efome and N. Li, *J. Membr. Sci.*, 2018, **555**, 78–87.
11 Y. S. Mahajan, A. K. Shah, R. S. Kamath, N. B. Salve and S. M. Mahajani, *Sep. Purif. Technol.*, 2008, **59**, 58–66.
12 A. Narebska and A. Warszawski, *J. Membr. Sci.*, 1994, **88**, 167–175.
13 F. Fu and Q. Wang, *J. Environ. Manage.*, 2011, **92**, 407–418.
14 B. Saha, S. P. Chopade and S. M. Mahajani, *Catal. Today*, 2000, **60**, 147–157.
15 A. T. Cherif, C. Gavach, T. Cohen, P. Dagard and L. Albert, *Hydrometallurgy*, 1988, **21**, 191–201.
16 G. Pourcelly, I. Tugas and C. Gavach, *J. Membr. Sci.*, 1994, **97**, 99–107.
17 Z. Wang, Y. Luo and P. Yu, *J. Membr. Sci.*, 2006, **280**, 134–137.
18 D. A. Vermaas, J. Veerman, M. Saakes and K. Nijmeijer, *Energy Environ. Sci.*, 2014, **7**, 1434–1445.
19 B. V. Bruggen, A. Koninckx and C. Vandecasteele, *Water Res.*, 2004, **38**, 1347–1353.
20 Y. Zhu, M. Ahmad, L. Yang, M. Misovich, A. Yaroshchuk and M. L. Bruening, *J. Membr. Sci.*, 2017, **537**, 177–185.
21 H. Farrokhzad, S. Darvishmanesh, G. Genduso, T. V. Gerven and B. V. D. Bruggen, *Electrochim. Acta*, 2015, **158**, 64–72.
22 L. X. Tuan, M. Verbanck, C. Buess-Herman and H. D. Hurwitz, *J. Membr. Sci.*, 2006, **284**, 67–78.
23 N. Li, D. S. Hwang, S. Y. Lee, Y. L. Liu, Y. M. Lee and M. D. Guiver, *Macromolecules*, 2011, **44**, 4901–4910.
24 S. J. Paddison, *Annu. Rev. Mater. Res.*, 2003, **33**, 289–319.
25 T. Sata, T. Funakoshi and K. Akai, *Macromolecules*, 1996, **29**, 4029–4035.
26 T. Sata, T. Sata and W. K. Yang, *J. Membr. Sci.*, 2002, **206**, 31–60.
27 T. Sata, R. Yamane and Y. Mizutani, *J. Polym. Sci., Part A: Polym. Chem.*, 1979, **17**, 2071–2085.
28 L. Ge, X. Liu, G. Wang, B. Wu, L. Wu, E. Bakangura and T. Xu, *J. Membr. Sci.*, 2015, **475**, 273–280.
29 B. Tong, C. Cheng and T. Xu, *Sep. Purif. Technol.*, 2017, **174**, 203–211.
30 L. Wang, F. Zhang, Z. Li, J. Liao, Y. Huang, Y. Lei and N. Li, *J. Membr. Sci.*, 2018, **549**, 543–549.
31 J. Ran, M. Hu, D. Yu, Y. He and T. Xu, *J. Membr. Sci.*, 2016, **520**, 630–638.
32 T. B. Norsten, M. D. Guiver, J. Murphy, T. Astill, T. Navessin, S. Holdcroft, B. L. Frankamp, V. M. Rotello and J. Ding, *Adv. Funct. Mater.*, 2006, **16**, 1814–1822.
33 M. Ingratta, E. P. Jutemar and P. Jannasch, *Macromolecules*, 2011, **44**, 2074–2083.
34 N. Li, C. Wang, S. Y. Lee, C. H. Park, Y. M. Lee and M. D. Guiver, *Angew. Chem., Int. Ed.*, 2011, **123**, 9324–9327.
35 N. Li and M. D. Guiver, *Macromolecules*, 2014, **47**, 2175–2198.
36 Y. Lin, X. Huang, R. Zheng, J. Lin, F. Ding and Q. Ling, *Chem. J. Chinese U.*, 2014, **35**, 633–638.
37 D. S. Kim, G. P. R. And and M. D. Guiver, *Macromolecules*, 2008, **41**, 2126–2134.
38 M. Tanaka, M. Koike, K. Miyatake and M. Watanabe, *Macromolecules*, 2010, **43**, 2657–2659.
39 Y. S. Kim, B. Einsla, M. Sankir, W. Harrison and B. S. Pivovar, *Polymer*, 2006, **47**, 4026–4035.
40 F. Sun, C. Wu, Y. Wu and T. Xu, *J. Membr. Sci.*, 2014, **450**, 103–110.
41 N. White, M. Misovich, A. Yaroshchuk and M. L. Bruening, *ACS Appl. Mater. Interfaces*, 2015, **7**, 6620–6628.
42 L. Bazinet, J. F. Poulin and J. Amiot, *Sep. Sci. Technol.*, 2007, **42**, 2501–2518.
43 L. Ge, B. Wu, Q. Li, Y. Wang, D. Yu, L. Wu, J. Pan, J. Miao and T. Xu, *J. Membr. Sci.*, 2016, **498**, 192–200.

44 S. P. Rannard, N. J. Davis and I. Herbert, *Macromolecules*, 2004, **37**, 9418–9430.
45 L. Lei, X. Zhu, J. Xu, H. Qian, Z. Zou and H. Yang, *J. Power Sources*, 2017, **15**, 41–48.
46 N. Li, Y. Leng, M. A. Hickner and C. Y. Wang, *J. Am. Chem. Soc.*, 2013, **135**, 10124–10133.
47 M. Zhang, C. Shan, L. Liu, J. Liao, Q. Chen, M. Zhu, Y. Wang, L. An and N. Li, *ACS Appl. Mater. Interfaces*, 2016, **8**, 23321–23330.
48 E. A. Weiber and P. Jannasch, *ChemSusChem*, 2014, **7**, 2621–2630.
49 C. Yang, L. Liu, X. Han, Z. Huang, J. Dong and N. Li, *J. Mater. Chem. A*, 2017, **5**, 10301–10310.
50 N. Li, T. Yan, Z. Li, T. Thurnalbrecht and W. H. Binder, *Energy Environ. Sci.*, 2012, **5**, 7888–7892.
51 M. Wang, X. Liu, Y. Jia and X. Wang, *Sep. Purif. Technol.*, 2015, **140**, 69–76.
52 Y. Tanaka, M. Iwahashi and M. Kogure, *J. Membr. Sci.*, 1994, **92**, 217–228.
53 M. C. Marti-Calatayud, D. C. Buzzi, M. Garcia-Gabaldon, A. M. Bernardes, J. A. S. Tenorio and V. Perez-Herranz, *J. Membr. Sci.*, 2014, **466**, 45–57.
54 J. J. Krol, M. Wessling and H. Strathmann, *J. Membr. Sci.*, 1999, **162**, 145–154.
55 C. Wang, N. Li, D. W. Shin, S. Y. Lee, N. R. Kang, Y. M. Lee and M. D. Guiver, *Macromolecules*, 2011, **44**, 7296–7306.
56 A. Volkov, S. Paula and D. Deamer, *Bioelectrochem. Bioenerg.*, 1997, **42**, 153–160.
57 M. J. Han and S. T. Nam, *J. Membr. Sci.*, 2002, **202**, 55–61.
58 K. W. Lee, B. K. Seo, S. T. Nam and M. J. Han, *Desalination*, 2003, **159**, 289–296.
59 Y. He, L. Ge, Z. Ge, Z. Zhao, F. Sheng, X. Liu, X. Ge, Z. Yang, R. Fu, Z. Liu, L. Wu and T. Xu, *J. Membr. Sci.*, 2018, **563**, 320–325.
60 F. Li, Y. Jia, T. Bai and M. Wang, *J. Membr. Sci.*, 2018, **564**, 267–274.
61 L. Ge, L. Wu, B. Wu, G. Wang and T. Xu, *J. Membr. Sci.*, 2014, **459**, 217–222.
62 M. F. S. Román, I. Ortiz-Gándara, E. Bringas, R. Ibañez and I. Ortiz, *Desalination*, 2018, **440**, 78–87.